Turkish Journal of Chemistry

http://journals.tubitak.gov.tr/chem/

Research Article

Turk J Chem
(2020) 44: 502 – 517
© TÜBİTAK
doi:10.3906/kim-1908-62

Combined computational and experimental studies on cysteine-sulfadiazine adduct formation

Nursel ACAR SELÇUKİ[1,*], **Emine COŞKUN**[2], **Ender BİÇER**[2]
[1]Department of Chemistry, Faculty of Science, Ege University, Bornova, İzmir, Turkey
[2]Department of Chemistry, Faculty of Arts and Science, Ondokuz Mayıs University, Atakum, Samsun, Turkey

Received: 31.08.2019 • **Accepted/Published Online:** 22.02.2020 • **Final Version:** 01.04.2020

Abstract: The electrochemical characterization of sulfadiazine-cysteine (SD-CYS) adduct formation was performed in phosphate buffer (pH 7) on the basis of voltammetric current and peak potential measurements. Due to the association of cysteine with sulfadiazine, the reduction peak currents of mercuric and mercurous cysteine thiolates decreased and their peak potentials simultaneously shifted to less negative potentials. By using the current changes of mercurous cysteine thiolate, it was determined that cysteine and sulfadiazine are associated with a 1:1 stoichiometry with a conditional association constant of 1.99 $\times 10^4$ M^{-1}. In addition to experimental studies, a computational approach was carried out to study the geometrical parameters, electron densities, and UV-Vis absorption spectra of sulfadiazine and SD-CYS adduct in water. Calculated (B3LYP/6-311++G(d,p) level) and experimental UV-Vis absorption spectra of the compounds were found to be in good agreement in water. The computational study suggests that cysteine bound to the C(5) on the pyrimidine ring via SH-group nucleophilic attack. Computational results reveal that sulfadiazine and its derivatives effectively bind cysteine and may lead to new molecules/drugs to target cysteine.

Key words: Cysteine-sulfadiazine adduct, nucleophilic attack, density functional theory

1. Introduction

Sulfadiazine (SD) is used for curing infections caused by gram-positive and gram-negative organisms [1] and it belongs to the sulfonamide category [2]. The sulfonamides are found in blood in three different forms: protein-bound, conjugated (acetylated and possibly others), and free [3]. The drug acts by the diffusion of its unbound form through the circulatory system and interacts with action sites [2].

Biological processes inside the human body are directly affected by drug–protein interactions [4]. Drug–protein interactions are usually investigated by using small molecular systems in which amino acids, peptides, and their derivatives are used to mimic proteins in aqueous solutions [4–7]. These simpler systems are more useful as they simplify the investigation of interactions in aqueous solutions by decreasing the number of functional groups in proteins [4]. Sulfadiazine and other sulfonamides are inhibitors of the enzyme dihydropteroate synthase (DHPS) [8,9].

There is great interest in biomedical research to take advantage of the various structural interactions between amino acids and antibiotics. However, some side reactions may cause problems. For example, when the substituent groups of drugs interact with amino acids, the drugs will not work properly, or drug–amino acid complexes may display different effects rather than the expected drug properties. Therefore, knowledge of the

*Correspondence: nursel.acar@ege.edu.tr

interactions between drugs and amino acids will give rise to ideas about drug design. Although there are other amino acids chosen as drug targets, the presence of a thiol group makes cysteine a primary research interest [10,11].

Cysteine (CYS) is one of the two sulfur-containing proteinogenic amino acids and is involved in some important cellular functions like detoxification, protein synthesis, and metabolism [12,13]. The sulfhydryl (-SH) group of CYS is essential for proteins' and enzymes' biological functions and it exists as thiol (-SH) or thiolate ($-S^-$) forms at neutral pH [12,13]. The acidity (K_a) of the thiol group regulates the equilibrium and hence the relative amount of S^- with respect to SH. Accordingly, pK_a for the sulfhydryl group of CYS is 8.30 [14]. At pH 7.0, both thiol and thiolate groups coexist in the medium; however, CYS probably reacts in its deprotonated form. The free energy cost for deprotonation depends on the pK_a and pH values [15–17]. Thus, for sulfadiazine-cysteine (SD-CYS) adduct formation, the pH of the medium was selected as 7.0. Also, CYS has been identified as a valuable biomarker [18]. There are therefore numerous research studies focused on the interactions of CYS with folates, catechol, quinoids, benzoquinones, and some drugs [18–29].

Although there are many studies on the interactions of SD with some compounds (cyclodextrins, glycine, leucine, aspartic acid, glutamic acid, arginine, human serum albumin, peptide amides, lysozyme, DNA, water-soluble proteins) [1–3,30–35], adduct formation between SD and CYS has not been addressed in the literature. Electrochemical techniques are frequently used to study the effects of electroactive species upon molecular interactions [36–38]. In the present study, the binding of SD to CYS was investigated in a neutral aqueous medium by means of square-wave voltammetry, UV-Vis spectroscopy, and computational studies together with optimized geometries. The current study focuses on covalent bonding between SD and CYS, which will provide useful information for the development of new molecules or drugs targeting CYS.

2. Materials and methods

2.1. Reagents and equipment

Square-wave voltammograms (SWVs) were recorded using an EG&G PAR 384B Polarographic Analyzer combined with the EG&G PARC 303A SMDE. The electrode system used consisted of a hanging mercury drop electrode (working electrode), $Ag/AgCl/KCl_{sat.}$ (reference electrode), and Pt wire (auxiliary electrode). ECD-SOFT software was used to obtain voltammograms on a laptop computer [39]. A Janway 3010 pH meter was used for all pH measurements. UV-Vis absorption spectra were obtained from a PerkinElmer Lambda 35 spectrophotometer. FTIR-ATR spectra were obtained by a PerkinElmer Spectrum 100 FT-IR Spectrometer.

L-CYS was purchased from Merck and SD was purchased from Sigma. All other reagents were of analytical reagent grade. SD was dissolved in methanol. Stock solutions of other reagents were prepared daily by dissolving their appropriate amounts in ultrapure water (specific resistivity: 18.2 MΩ cm). Phosphate buffer was also prepared in ultrapure water and its pH (pH 7.0) was adjusted by addition of 0.5 M NaOH solution.

2.2. Synthesis of SD-CYS complex

A mixture of 0.0001 mol SD and 0.0001 mol L-CYS was dissolved in 30 mL of methanol (70%). This solution was continuously stirred with a constant temperature about 40 °C for 4 h. After the evaporation of most of the solvent at room temperature for 4–5 weeks, a white solid compound (SD-CYS adduct) was obtained and dried at room temperature. The simplified reaction is given in Figure 1.

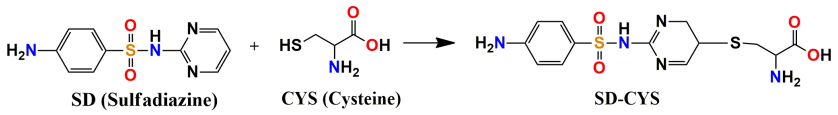

Figure 1. Molecular structures and reaction scheme of the investigated compounds.

2.3. Electrochemical procedure

Phosphate buffer (10 mL, 0.02 M, pH 7.0) was added to the electrochemical cell and degassed with N_2 for 300 s. The voltammogram was recorded by applying the potential scan toward the positive direction. After the background voltammogram was obtained, CYS was added and the voltammogram was obtained by the same procedure. Appropriate amounts of SD were then added to the electrochemical cell and the changes were followed in voltammograms. All electrochemical experiments were carried out at room temperature.

2.4. Computational details

Spartan08 [40] was used to obtain initial structures by conformational analysis. The geometry optimizations were performed with Gaussian09 [41] using density functional theory (DFT) [42–44] with the ωB97XD functional [45] in combination with the 6-311++G(d,p) basis set. This functional was chosen as it has long-range terms and can calculate weak dispersion interactions [45]. Gaussview5.0 [46] was used for visualization. The minimum nature of all optimized structures was verified with frequency calculations at the same level. Time-dependent DFT (TD-DFT) calculations were performed to calculate the UV-Vis absorption spectra (N = 100 states) and molecular orbital energies (E_{HOMO}, E_{LUMO}, ΔE_{H-L}) using the ground-state optimized geometries. All TD-DFT calculations were performed with Becke's 3-parameter exchange and Lee–Yang–Parr correlation functionals (B3LYP) [47] in combination with the 6-311++G(d,p) basis set. TD-DFT computations were repeated with the ωB97XD functional with the same basis set to obtain UV-Vis spectra and both computational results were compared with experimental UV-Vis absorption spectra. To mimic the real systems, all calculations were done in solution. The polarizable continuum model (PCM) [48] was used in all DFT and TD-DFT calculations to investigate solvent effects on the electronic transitions in solution (water).

3. Results and discussion

3.1. Voltammetry measurements

The nucleophilic substitution reaction of CYS on SD was studied by square-wave voltammetry. Figure 2 shows the square-wave voltammogram of 1.0 $\times 10^{-4}$ M SD in phosphate buffer solution of pH 7. As can be seen in Figure 2, SD shows two cathodic peaks at –0.396 (1U) and –1.500 V (2U), corresponding to the reduction of Hg(II)-sulfadiazine adsorbed on the mercury electrode [49,50] and the reduction at the Ar-SO_2NH- group in a single irreversible reduction step [51–53], respectively.

On the other hand, square-wave voltammograms obtained from 1.0 $\times 10^{-5}$ M CYS in the absence and presence of SD are shown in Figure 3. In the phosphate buffer solution of pH 7, CYS gave two well-developed cathodic peaks in the absence of SD (Figure 3). These peaks at –0.190 and –0.766 V (Figure 3) can be explained by the reductions of mercuric (1U) and mercurous cysteine thiolates (3U), respectively [54,55].

Upon addition of SD, the reduction potentials of the mercuric and mercurous thiolates shifted positively and their cathodic peak currents started to decrease (Figure 3), which suggested the nucleophilic attack of CYS

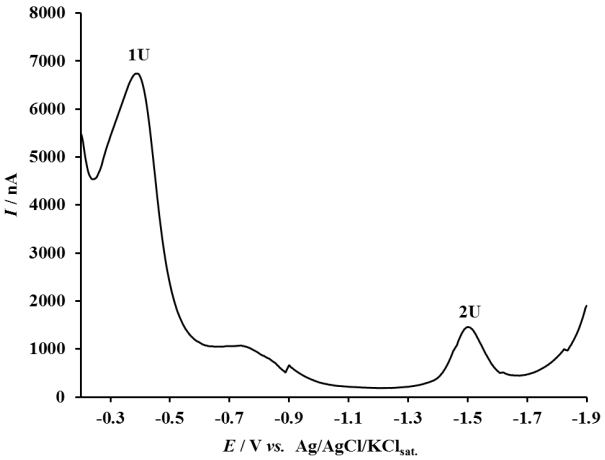

Figure 2. SWV of 1.0 $\times 10^{-4}$ M SD in phosphate buffer solution of pH 7.0 (other experimental conditions: equilibrium time of 5 s, scan increment of 4 mV, and frequency of 120 Hz).

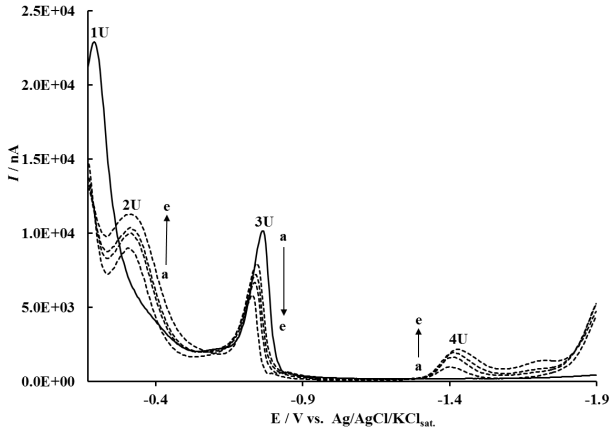

Figure 3. SWVs of 1.0 $\times 10^{-5}$ M CYS in the presence of a) 0, b) 1.0 $\times 10^{-4}$, c) 2.8 $\times 10^{-4}$, d) 3.6 $\times 10^{-4}$, and e) 6.0 $\times 10^{-4}$ M SD in phosphate buffer solution of pH 7.0 (other experimental conditions: equilibrium time of 5 s, scan increment of 4 mV, and frequency of 120 Hz).

to SD, or in other words the formation of the SD-CYS adduct. At the same time, upon addition of SD to CYS solution, newly appeared cathodic peaks at –0.342 (2U) and –1.426 V (4U) were increased gradually (Figure 3). New cathodic peaks (2U and 4U in Figure 3) correspond to the reductions of mercury salt and the electroactive Ar-SO_2NH- group of the SD-CYS adduct at less negative potentials than those of free SD. This behavior is in agreement with that reported by Proková and Heyrovský for thiols and their folate adducts [19].

According to the decrease in the peak current of mercurous cysteine thiolate with increasing concentrations of SD (Figure 3), the binding constant was calculated according to the following equation [56]:

$$[\mathrm{SD}]^{-1} = K\ (1 - A)\ [1 - (I / I_o)]^{-1} - K,$$

where K is the binding constant, I_o and I are the peak currents in the absence and presence of SD, and A is the proportionality constant. The plot of $[\mathrm{SD}]^{-1}$ versus $[1 - (I / I_o)]^{-1}$ was drawn (Figure 4) and the value of K is calculated as 1.99 $\times 10^4$ M^{-1} (R^2 = 0.9855) using the intercept from this graph. The calculated association constant of 1.99 $\times 10^4$ M^{-1} is attributed to a reversible inhibition [57] and a moderate-strength interaction [58]. The irreversible inhibition process is controlled by the barrier height: for a sufficiently high barrier the crossing is slower than the duration of the experiment. If the whole enzyme is taken into account, use of the simplified EVB model is particularly effective in cases with high barriers and many protonation sites in a computational approach [59].

It is well known that a SH-group may be added to the pyrimidine C(5) = C(6) bond by the CYS nucleophilic attack on the substrate [60]. Also, the interaction of thiyl radicals with the C5-C6 double bond in pyrimidines was reported by Wójcik et al. [61]. Moreover, it was observed that at the formation of uracil-CYS heterodimer, the amino acid was added to the 5 position rather than the 6 position of uracil with the formation of 5-S-cysteine-6-hydrouracil [62]. In this study, we also suggest that the SD-CYS adduct comes from the nucleophilic attack of the SH group of CYS to the C(5) = C(6) bond of pyrimidine at the SD molecule.

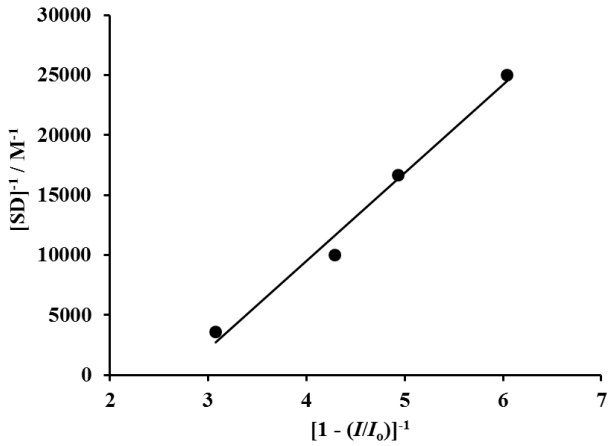

Figure 4. Plot of $[SD]^{-1}$ vs. $[1 - (I/I_o)]^{-1}$ for SD-CYS adduct.

3.2. ATR-FTIR study

The infrared spectra of SD, CYS, and SD-CYS adducts are shown in Figure 5. Figure 6 displays the optimized geometries of the reactants and the product; selected important bonds and atoms are numbered for simplification. The characteristic bands of SD (Figure 5) are seen at 3422 and 3353 cm^{-1} for symmetric stretching and asymmetric stretching of NH_2 ($v_s(NH_2)$ and $v_{as}(NH_2)$). In the 2750–3150 cm^{-1} region of the spectrum, there are C-H stretching bands (Figure 5). A new peak in the same region appeared at 2819 cm^{-1} (Figure 5, bond 5) for symmetrical vibration of CH_2 ($v_s(CH_2)$) due to pyrimidine deformation. The bands at 1575, 1490, 1440, and 1410 cm^{-1} are ring skeletal vibrations. The bands at 1325 and 1150 cm^{-1} belong to the -SO_2-N-group. The bands at 1585 and 1621 cm^{-1} are assigned to $v_{C=N}$ [1,63]. The new peaks are observed at 1383 and 1298 cm^{-1}. The peak observed at 2543 cm^{-1} in the ATR-FTIR spectrum of CYS (Figure 5) is due to the SH stretching [64–66]. Since this peak is not observed in the ATR-FTIR spectrum of the SD-CYS adduct (Figure 5), this observation may lead to the conclusion that the thiol hydrogen atom moved to the C5-C6 double bond on SD. Moreover, some important differences were observed in the ATR-FTIR spectrum of the SD-CYS adduct. In the range of 3500–2750 cm^{-1}, although the bands are similar, mainly decreases in intensity and small variations in position were obtained.

3.3. Computational results

Free CYS represents only truncated protein. However, by considering the entire enzyme, properties, and especially kinetics, would be changed (the rate constant will probably increase relative to the corresponding reaction in aqueous solution). Multiscale ab initio QM/MM is typically computationally too demanding and does not allow for well-converged reaction profiles. Empirical valence bond (EVB) is a method developed for calculating free energies of activation for enzyme reactions and reactions in solution [67]. In the current study, a simple mechanism for the reaction of free CYS with SD is investigated and the free energy values are calculated by DFT and PCM methods as explained in Section 2.

There are two possible sites for the complex formation reaction between SD and CYS. The first is between the SH group of CYS and the pyrimidine of SD (S-bridged structure previously explained), and the second is between the carbonyl group of CYS and the phenyl-NH_2 group of SD. Approximately, 100 conformers for both

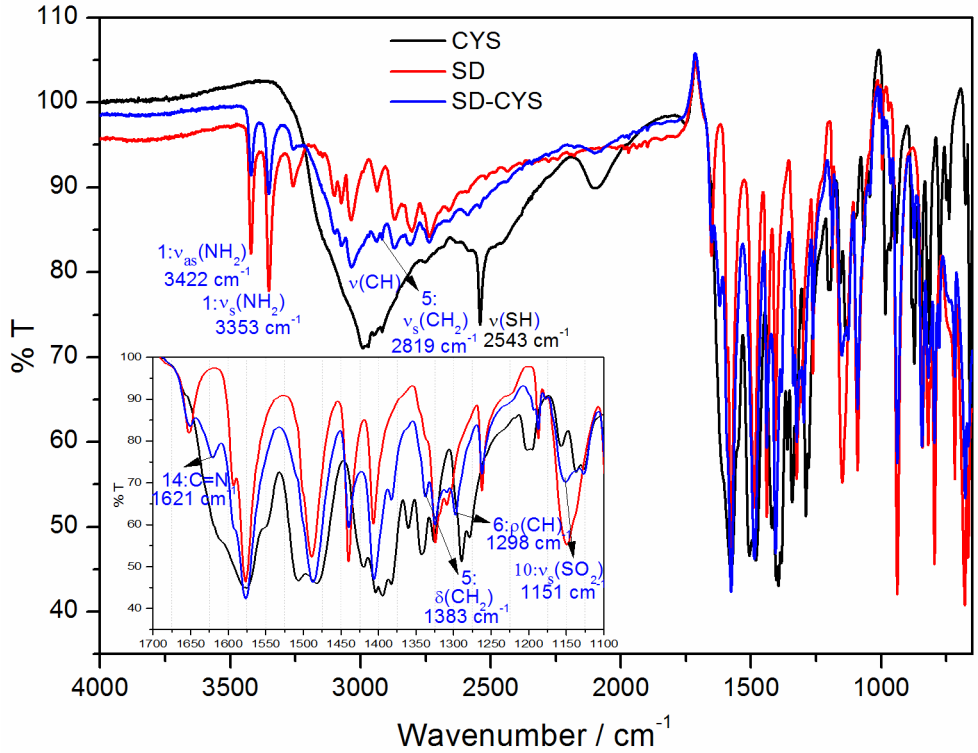

Figure 5. Experimental FTIR spectra of the investigated compounds (frequencies between 1100 and 1700 cm^{-1} are shown separately and important frequencies for SD-CYS complex are written).

possibilities were optimized in water. Table S1 in the Supplemental Information displays E+ZPE energies and the optimized geometry of the most stable NH_2-bridged SD-CYS complex in water. The results for the SH-bridged SD-CYS complex are given in Table S2 in gas phase and in water. Computational results revealed that the SH binding site forms the most stable complex, in agreement with experimental results. The NH_2-bridged complex forms in a condensation reaction producing 1 mol of water as a second product. Therefore, summed energies of the NH_2-bridged complex and water are compared with the energy of the S-bridged complex. As seen from Tables S1 and S2, the S-bridged complex is more stable than the NH_2-bridged complex and this confirms the experimentally observed structure. The optimized geometries of the most stable structures for the reactants and product are shown in Figure 6.

Table 1 lists the total energy and free energy differences of the investigated molecules for the reaction given in Figure 1. Table S3 shows dipole moments (μ, in debyes), sum of total electronic energies and zero point energies (E+ZPE), and selected dihedral angles of SD and SD-CYS for ground-state geometries optimized at the ωB97XD/6-311++G(d,p) level of theory in water. Dipole moment of the complex increased significantly with the inclusion of NH_2 and OH groups from CYS. Bond distances changed slightly in the complex compared to the initial monomers. The S2-C7-C8 angle (114.12°) decreased by 4.37°in the complex compared to CYS. On the other hand, dihedral angles show significant differences between SD and SD-CYS molecules. Another important change is the distortion of the planarity for the pyrimidine ring in SD because of the newly formed S-C bond. The first step of the reaction is the formation of INT and it has a free energy barrier of 22 kcal/mol (Table 1; Figure S1). The transition state (TS1) is a late transition state and is isoenergetic with the INT. These

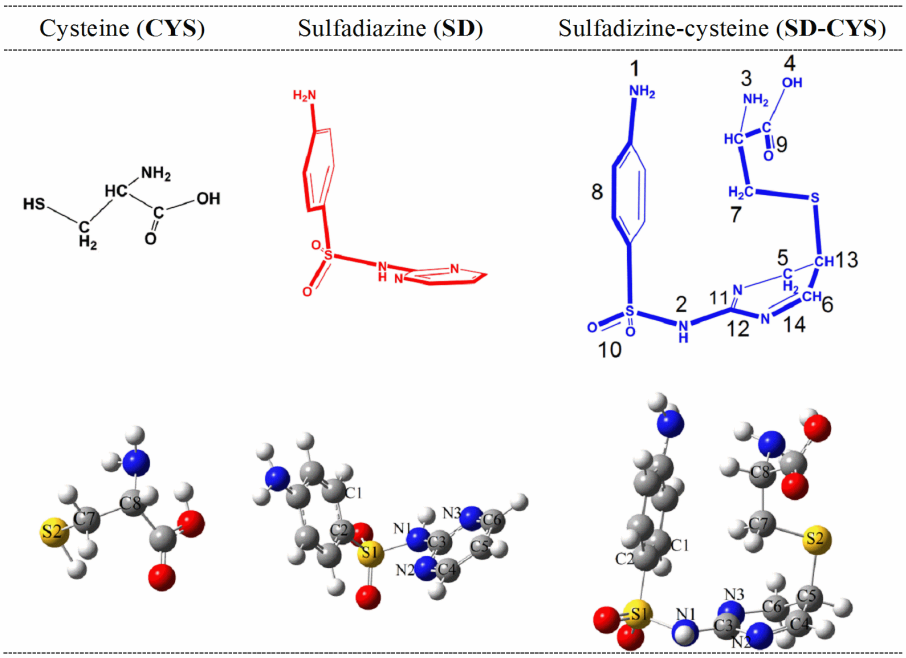

Figure 6. Optimized geometries of the investigated molecules in water at ωB97XD/6- 311++G(d,p) level.

energy values indicate that this step is reversible. The second step is the formation of the product (SD-CYS adduct) with the addition of H cation to the pyrimidine ring. The transition state (TS2) for this step could not be obtained even though all available options in Gaussian09 were used. This step is highly exergonic and the product is more stable than the INT by 190 kcal/mol. The second step is irreversible and once the product is stable the reaction terminates.

Table 1. Calculated electronic and free energy differences for the reaction of SD and CYS at wB97XD/6-311++G(d,p) level.

	E+ZPE (Hartree)	E+ΔG (Hartree)	^{a}ΔE (kcal/mol)	^{b}ΔΔG (kcal/mol)	Distances (Å) (C.....S)
Reactants (SD+CYS)	–1875.84072	–1875.91625	0.00	0.00	
TS1	–1875.82947	–1875.88075	7.06	22.28	2.038
INT	–1875.82780	–1875.87993	8.10	22.79	1.978
product	–1876.29516	–1876.34765	–190.01	–190.23	1.872

^{a}: ΔE = [E+ZPE(SD-CYS) – E+ZPE(SD) – E+ZPE(CYS)].
^{b}: ΔΔG = [E+ΔG(SD-CYS) – E+ΔG(SD) – E+ΔG(CYS)].

Calculated IR spectra of the investigated molecules are displayed in Figure 7. Selected stretching vibrations are shown in the figure for the molecules. With addition of CYS to the pyrimidine part of the SD molecule, the S-H stretching vibration (2739 cm^{-1}) of CYS disappeared and new vibrations appeared in the complex SD-CYS formation. Selected vibrational frequencies of the investigated molecules are given in Table S4 in detail. Some experimental vibrational bands are also included for comparison. New vibrations due to the distortions in pyrimidine at 3040 cm^{-1} and 3113 cm^{-1} appeared in the SD-CYS complex, corresponding to

CH_2 symmetrical ($v_s(CH_2)$) and asymmetrical ($v_{as}(CH_2)$) vibrations, respectively. These peaks agree quite well with the peak observed at 2819 cm^{-1} experimentally. Computed v(C=N) peaks at 1756 cm^{-1} and 1698 cm^{-1} also agree with experimentally observed peaks at 1621 cm^{-1} and 1585 cm^{-1}. Additionally, computed vibrational peaks in the same region of the molecule at 1478 cm^{-1} $\delta(CH_2)$ and 1326 cm^{-1} ρ(C-H) are in agreement with experimentally observed peaks at 1383 cm^{-1} and 1298 cm^{-1}.

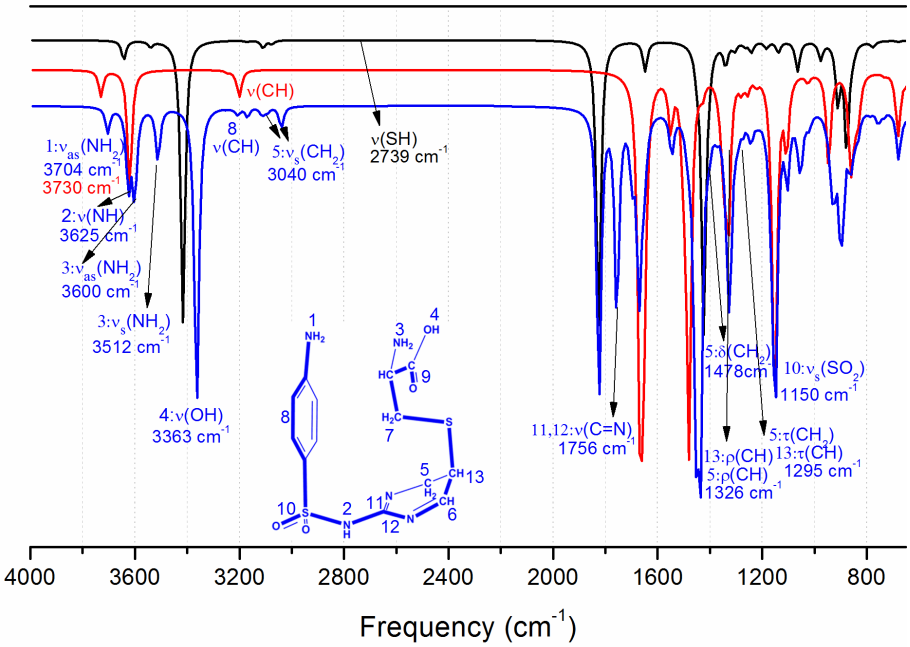

Figure 7. Calculated IR spectra of CYS, SD, and SD-CYS complex at ωB97XD/6-311++G(d,p) level.

Observed peaks in the calculated and experimental IR spectra display shifts for the frequencies for the same vibrations as computational vibrational frequencies were not scaled. Another reason for the observed shifts may be that the experimental measurements were taken in the solid state, whereas computations were performed in solution. Although there are shifts in the IR peak values, the peaks with the same nature confirm that the formed complex has a S-bridged structure as experimentally predicted.

We focus on the frontier HOMO and LUMO orbitals for determining chemical stability. Koopmans' theorem [68] states that the ionization potential (IP) and electron affinity (EA) are related to the orbital energies of HOMO and LUMO: EA: $-E_{LUMO}$; IP: $-E_{HOMO}$. Those molecular orbitals and orbital energy gaps of SD and SD-CYS were calculated at the B3LYP/6-311++G(d,p) level and are given in Figure 8.

The HOMO-LUMO gaps are larger in hard compounds and they are more stable and less reactive than in soft compounds with smaller HOMO-LUMO gaps. A small HOMO-LUMO gap allows transitions to excited states more easily; therefore, the electron density of soft molecules will change more easily compared to hard molecules. The conceptual DFT approach can provide information on molecular structure stability and reactivity [69].

Additionally, the absolute softness (σ), chemical hardness (η), and absolute electronegativity (χ) of the molecules were calculated at the same level and are listed in Table 2. The chemical hardness is a good indicator of chemical stability and can be used as a measure for the stability and reactivity of chemical compounds.

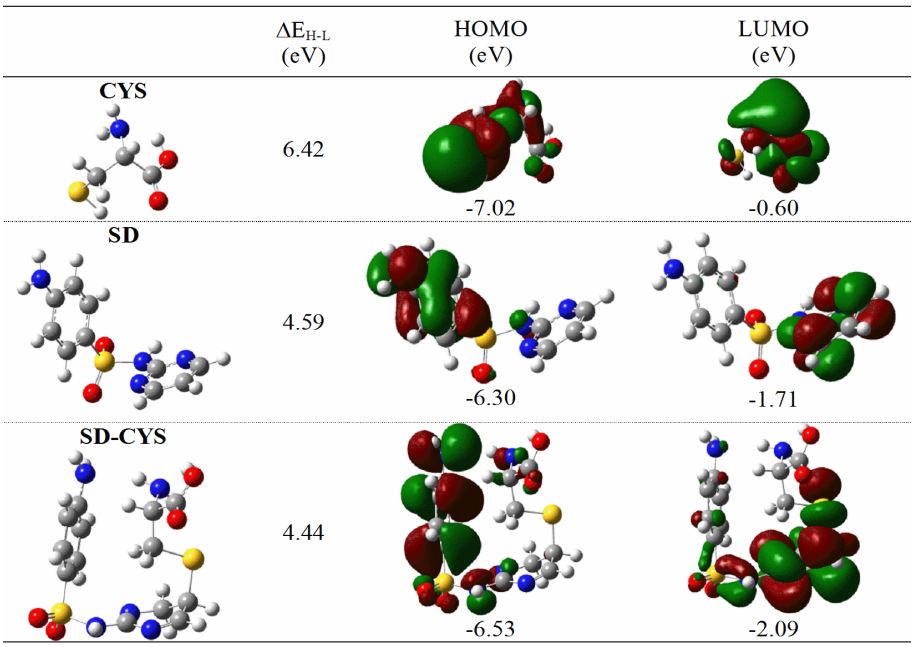

Figure 8. Frontier molecular orbitals, their energies, and HOMO-LUMO energy gaps for the compounds CYS, SD, and SD-CYS calculated at B3LYP/6-311++G(d,p) level in water.

As a rule of thumb, soft molecules are more polarizable than hard ones. The absolute electronegativity (χ) [70], chemical hardness (η) [71–73], and absolute softness were obtained by using the formulae $\chi = (\mathrm{IP} + \mathrm{EA})/2$, $\eta = (\mathrm{IP} - \mathrm{EA})/2$, and $s = 1/\eta$, respectively. In addition, the electrophilicity index [74] (ω, global reactivity descriptor of molecules, as $\mu^2/2\eta$, where μ is the chemical potential: $\mu = -(\mathrm{IP} + \mathrm{EA})/2$) [75] was calculated. In general, the electrophiles have a tendency to accept electrons and may form bonds with nucleophiles. Thus, electrophilicity is also a useful depicter for the analysis of chemical reactivity.

Table 2. Frontier orbital energies, HOMO-LUMO energy gap (ΔE_{H-L}), ionization potential (IP), electronic affinity (EA), absolute electronegativity (χ), chemical hardness (η), absolute softness (σ), chemical potential (μ), and electrophilicity index (ω) of CYS, SD, and SD-CYS for ground-state geometries in water calculated at B3LYP/6-311++G(d,p) level.

	CYS	SD	SD-CYS
E_{HOMO} (eV)	–7.02	–6.29	–6.53
E_{LUMO} (eV)	–0.60	–1.71	–2.09
ΔE_{H-L} (eV)	6.42	4.58	4.44
IP (eV)	7.02	6.29	6.53
EA (eV)	0.60	1.71	2.09
χ (eV)	3.81	4.00	4.31
η (eV)	3.21	2.29	2.22
σ (eV^{-1})	0.31	0.44	0.45
μ (eV)	–3.81	–4.00	–4.31
ω (eV)	2.26	3.57	4.18

CYS and SD have higher stability and chemical hardness than SD-CYS under high excitation energies. The IP values of the SD-CYS molecule are not the lowest, but with the addition of cysteine to SD, the electron affinity of the SD-CYS system increases. The electrophilicity index of the complex is the highest.

UV-Vis absorption spectra of SD (5.2×10^{-5} M) and SD-CYS (1.9×10^{-3} M) in water were obtained experimentally and computationally with time-dependent density functional theory (TD-DFT) and the spectra are presented in Figure 9. Figure 10 shows the differences of UV-Vis absorption spectra between the calculated spectra with different functionals (B3LYP and ωB97XD) and the experimental one. B3LYP results are used in discussion as they agree better with the experimental spectra.

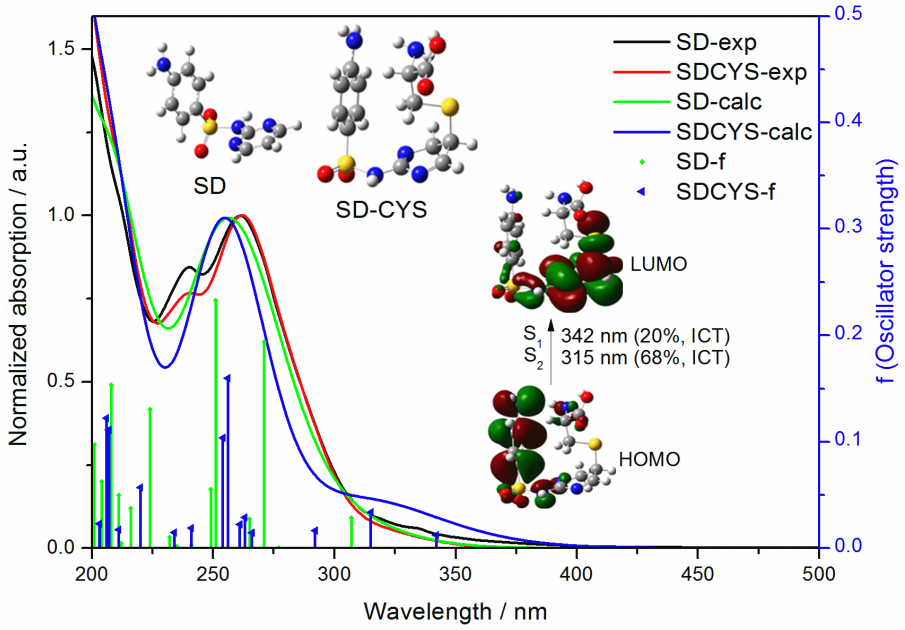

Figure 9. Experimental and calculated UV-Vis absorption spectra of SD and SD-CYS in water.

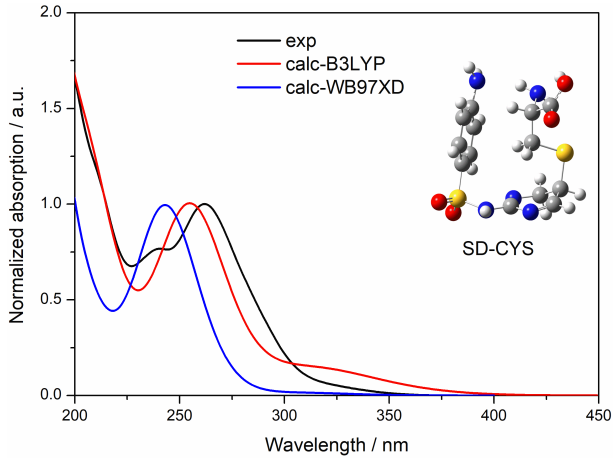

Figure 10. Comparison of experimental and calculated (with different functionals) UV-Vis absorption spectra of SD-CYS in water.

Calculated wavelengths in water are given in Table 3 for SD-CYS and Table S5 for SD in detail. Comparing the $S_0 \rightarrow S_1$ wavelengths of SD and SD-CYS in water, a red shift of 35 nm was observed. The long wavelength absorption peak (342 nm) of the SD-CYS complex belongs to the transition between HOMO/HOMO-1 and LUMO orbitals, and it has an intramolecular charge transfer from aniline to pyrimidine and local excitation of pyrimidine characters. SD has S_1 transition at 307 nm, which is assigned to the intramolecular charge transfer between aniline and pyrimidine parts (ICT1) between HOMO and LUMO (Figure S2).

Table 3. Excitation energies (ΔE), wavelengths (λ_{ex}), transition dipole moments (μ_{tr}), oscillator strengths (f), excitation character, and involved transition molecular orbitals and their contributions for SD-CYS in water at B3LYP/6-311++G(d,p) level.

State	ΔE (eV)	λ_{ex} (nm)	μ_{tr} (D)	f	Character[a]	Predominant transitions	%
S_1	3.62	342	0.1379	0.0122	LE1 ICT1	H-1→L H→L	64 20
S_2	3.93	315	0.3510	0.0338	ICT1 LE1	H→L H-1→L	68 20
S_3	4.25	292	0.1590	0.0165	LE1,ICT1 LE1	H-2→L H-4—L	54 38
S_4	4.66	266	0.1275	0.0146	LE1 ICT1,LE1	H-4→L H-2→L	50 38
S_5	4.72	263	0.2499	0.0289	LE(phenyl) ICT3	H→L+2 H-3→L	50 33
S_6	4.76	261	0.1928	0.0225	ICT3 LE2	H-3→L H→L+1	60 20
S_7	4.85	256	1.3452	0.1598	LE2 LE1	H→L+1 H-1→L+1	52 32
S_8	4.89	254	0.8659	0.1037	LE1 LE2	H-1→L+1 H→L+1	59 34
S_{10}	5.15	241	0.1499	0.0189	ICT2	H-1→L+2	69
S_{26}	5.99	207	0.7585	0.1113	ICT4,LE1 ICT5,LE3	H-8→L H-5→L+1	48 29
S_{28}	6.03	206	0.8272	0.1222	ICT5,LE3 ICT4,LE1	H-5→L+1 H-8→L	46 24
S_{30}	6.10	203	0.1539	0.0230	ICT6	H-1→L+5	55

[a] ICT1: Intramolecular charge transfer from aniline to pyrimidine part; LE1: local excitation of pyrimidine part; LE2: local excitation of aniline; ICT2: intramolecular charge transfer from pyrimidine part to aniline; ICT3: intramolecular charge transfer from CYS and phenyl to pyrimidine part; ICT4: intramolecular charge transfer from CYS and aniline to pyrimidine; ICT5: intramolecular charge transfer from CYS to aniline; ICT6: intramolecular charge transfer from pyrimidine part and S to CYS.

In contrast to SD, SD-CYS displayed ICT1 at 315 nm (S_2 transition) between HOMO and LUMO orbitals, too. The absorption peaks observed at long wavelengths (342 nm, 315 nm) belong to the charge transfer from aniline to pyrimidine; unfortunately, these peaks do not appear in the experimental spectra as their oscillator strength values are too small. Experimental and calculated peaks at 260 nm can be local excitation of aniline (LE2). The significant peak of **SD** at 240 nm observed in the experimental UV spectrum was described as local excitation of pyrimidine (LE1) by computational results. CYS has its absorption band at wavelengths shorter

than 250 nm; therefore, its effect at longer wavelengths is not significant (spectra are not shown). Due to the U shape of SD-CYS, CYS and the NH_2 group at the opposite terminal are close to each other (distance between N in CYS and N in aniline = 3.22 Å). As a result, it has contributions to electronic transitions of SD-CYS at 207 and 206 nm (calculated) in the form of intramolecular charge transfer from cysteine to aniline part (ICT5). Additionally, there are other intramolecular charge transfers including cysteine: from CYS and phenyl to the pyrimidine part (ICT3, 261 nm), from CYS and aniline to the pyrimidine part (ICT4, 207 nm), and from the pyrimidine part and S to CYS (ICT6, 203 nm).

3.4. Conclusions

In this study, adduct formation between SD and CYS was confirmed by experimental and computational methods. Voltammetric measurements showed positive shifting at the peak potential of mercurous cysteine thiolate in the presence of SD, which revealed that a product formed from the fast follow-up reaction. Depending on the reactants and confirmed product, a reaction mechanism in which the CYS thiol group is added to the C(5) = C(6) double bond of the pyrimidine on SD by a nucleophilic attack is suggested.

DFT results have revealed that the S-bridged SD-CYS complex is more stable than the NH_2-bridged complex, as predicted by experimental results. Structural, electronic, and spectroscopic properties of the SD-CYS complex were calculated by using DFT and TD-DFT methods and the results were in quite good agreement with the experimental results. The calculated electrophilicity index of the complex is the highest among all studied systems. The calculated ΔE and $\Delta\Delta G$ values indicate that the adduct formation reaction is endergonic and requires energy, in agreement with the experimental procedure. Computations also indicate that SD and its derivatives may effectively bind CYS and can be used to develop new molecules/drugs to target CYS.

Acknowledgment

The authors are grateful to TÜBİTAK-ULAKBIM TRUBA and the Fen Cluster of the Ege University Faculty of Science for computer time.

References

1. Delrivo A, Zoppi A, Longhi MR. Interaction of sulfadiazine with cyclodextrins in aqueous solution and solid state. Carbohydrate Polymers 2012; 87: 1980-1988. doi: 10.1016/j.carbpol.2011.10.025
2. Ali MS, Al-Lohedan HA. Interaction of human serum albumin with sulfadiazine. Journal of Molecular Liquids 2014; 197: 124-130. doi: 10.1016/j.molliq.2014.04.029
3. Islam MM, Sonu VK, Gashnga PM, Moyon NS, Mitra S. Caffeine and sulfadiazine interact differently with human serum albumin: a combined fluorescence and molecular docking study. Spectrochimica Acta Part A 2016; 152: 23-33. doi: 10.1016/j.saa.2015.07.051
4. Sawhney N, Kumar M, Sandarve, Sharma P, Sharma AK et al. Structure-making behaviour of L-arginine in aqueous solution of drug ketorolac tromethamine: volumetric, compressibility and viscometric studies. Physics and Chemistry of Liquids 2018; 57: 184-203. doi: 10.1080/00319104.2018.1437918.
5. Banipal TS, Kaur J, Banipal PK, Singh K. Study of interactions between amino acids and zinc chloride in aqueous solutions through volumetric measurements at T = (288.15 to 318.15) K. Journal of Chemical and Engineering Data 2008; 53: 1803-1816. doi: 10.1021/je8001464
6. Pal A, Soni S. Volumetric approach to the interaction of diglycine in aqueous solutions of sulpha drugs at T = 288.15–308.15 K. Fluid Phase Equilibria 2012; 134: 144-151. doi: 10.1016/j.fluid.2012.08.001

7. Nain AK, Chand D. Volumetric, ultrasonic, and viscometric behaviour of glycine, dl-alanine, and l-valine in aqueous 1,4-butanediol solutions at different temperatures. Journal of Chemical Thermodynamics 2009; 41: 243-249. doi: 10.1016/j.jct.2008.09.008
8. Thomson JG, Cook M, Guttman M, Smith J, Thilmony R. Novel sul I binary vectors enable an inexpensive foliar selection method in Arabidopsis. BMC Res Notes 2011; 4: 44 doi: 10.1186/1756-0500-4-44
9. Voeller D, Kovacs J, Andrawis V, Chu E, Masur H et al. Interaction of *Pneumocystis carinii* dihydropteroate synthase with sulfonamides and diaminodiphenyl sulfone (dapsone). Journal of Infectious Diseases 1994; 169: 456-459. doi: 10.1093/infdis/169.2.456
10. Krenske EH, Petter RC, Houk KN. Kinetics and thermodynamics of reversible thiol additions to mono- and deactivated Michael acceptors: implications for the design of drugs that bind covalently to cysteines. Journal of Organic Chemistry 2016; 81: 11726-11733. doi: 10.1021/acs.joc.6b02188
11. Abhishek S, Sivadas S, Satish M, Deeksha W, Rajakumara E. Dynamic basis for auranofin drug recognition by thiol-reductases of human pathogens and intermediate coordinated adduct formation with catalytic cysteine residues. ACS Omega 2019; 4: 9593-9602. doi: 10.1021/acsomega.9b00529
12. Burtis CA, Ashwood ER. Tietz Fundamentals of Clinical Chemistry (4th Ed.). Philadelphia, PA, USA: WB Saunders, 1996.
13. Wang LH, Huang WS. Electrochemical oxidation of cysteine at a film gold modified carbon fiber microelectrode its application in a flow-through voltammetric sensor. Sensors 2012; 12: 3562-3577. doi: 10.3390/s120303562
14. Aldini G, Altomare A, Baron G, Vistoli G, Carini M et al. N-Acetylcysteine as an antioxidant and disulphide breaking agent: the reasons why. Free Radical Research 2018; 52:751–762. doi: 10.1080/10715762.2018.1468564
15. Stivers JT, Abeygunawardana C, Mildvan AS, Hajipour G, Whitman CP. 4-Oxalocrotonate tautomerase: pH dependence of catalysis and pKa values of active site residues. Biochemistry 1996; 35: 814-823. doi: 10.1021/bi9510789
16. Sham YY, Chu ZT, Warshel A. Consistent calculations of pKa's of ionizable residues in proteins: semi-microscopic and microscopic approaches. Journal of Physical Chemistry B 1997; 101: 4458-4472. doi: 10.1021/jp963412w
17. Repic M, Purg M, Vianello R, Mavri J. Examining electrostatic preorganization in monoamine oxidases A and B by structural comparison and pKa calculations. Journal of Physical Chemistry B 2014; 118: 4326-4332. doi: 10.1021/jp500795p
18. White PC, Lawrence NS, Tsai YC, Davis J, Compton RG. Electrochemically driven derivatisation-detection of cysteine. Microchimica Acta 2001; 137: 87-91. doi: 10.1007/s006040170
19. Proková B, Heyrovský M. Voltammetric evidence of interfacial interactions between folates and thiols. Bioelectrochemistry and Bioenergetics 1996; 41: 209-212. doi: 10.1016/S0302-4598(96)05099-4.
20. Heyrovský M, Proková B. Heterogeneous physico-chemical interactions following electrode reaction: interaction of folates with thiols. Collection of Czechoslovak Chemical Communications 1997; 62: 172-184. doi: 10.1135/cccc19970172
21. Lawrence NS, Davis J, Compton RG, Compton RG. Electrochemical detection of thiols in biological media. Talanta 2001; 53: 1089-1094. doi: 10.1016/S0039-9140(00)00579-8
22. Hignett G, Threlfell S, Wain AJ, Lawrence NS, Wilkins SJ et al. Electroanalytical exploitation of quinone–thiol interactions: application to the selective determination of cysteine. Analyst 2001; 126: 353-357. doi: 10.1039/B008616I
23. White PC, Lawrence NS, Davis J, Compton RG. Electrochemically initiated 1,4 additions: a versatile route to the determination of thiols. Analytica Chimica Acta 2001; 447: 1-10. doi: 10.1016/S0003-2670(01)01297-1.
24. White PC, Lawrence NS, Davis J, Compton RG. Electrochemical determination of thiols: a perspective. Electroanalysis 2002; 14: 89-98. doi: 10.1002/1521-4109(200201)14:2<89::AID-ELAN89>3.0.CO;2-Y

25. Biçer E, Çetinkaya P. A voltammetric study on the interaction of novobiocin with cysteine: pH effect. Journal of the Chilean Chemical Society 2009; 54: 46-50. doi: 10.4067/S0717-97072009000100011
26. Biçer E, Coşkun E. Voltammetric study of the interaction between oxacillin sodium and cysteine in the presence and absence of Mn(II) ions in neutral buffer solution. Journal of the Serbian Chemical Society 2007; 72: 1003-1013. doi: 10.2298/JSC0710003B
27. Çınar E, Biçer E. Voltammetric and spectroscopic studies on the interaction of pentoxifylline with cysteine in the presence and absence of UV irradiation. Zeitschrift für Physikalische Chemie 2005; 219: 817-830. doi: 10.1524/zpch.219.6.817.65709
28. Biçer E, Özdemir N. In vitro study of the interaction of cysteine with a thiazide diuretic (hydrochlorothiazide) at different pH by voltammetric and spectroscopic techniques. Russian Journal of Electrochemistry 2013; 49: 948-954. doi: 10.1134/S1023193513100042
29. Biçer E, Nuertayi P. Voltammetric, spectroscopic and thermal investigations of the interaction of levofloxacin with cysteine at physiological pH. Russian Journal of Electrochemistry 2017; 53: 469-478. doi: 10.1134/S1023193517050044
30. Delrivo A, Zoppi A, Granero G, Longhi M. Studies of ternary systems of sulfadiazine with β-cyclodextrin and amino acids. Ars Pharmaceutica 2016; 57: 167-176. doi: 10.4321/S2340-98942016000400003
31. Yiwei W, Xiaoqin Z, Jun D, Song H, Jianmin G. Studies on interactions between sulfadiazine and peptide amides. Biotechnology 2015; 14: 233-240. doi: 10.3923/biotech.2015.233.240
32. Sonu VK, Rajkumar I, Bhattacharjee K, Joshi SR, Mitra S. Interaction of caffeine and sulfadiazine with lysozyme adsorbed at colloidal metal nanoparticle interface: influence on drug transport ability and antibacterial activity. Journal of Biomolecular Structure and Dynamics 2018; 36: 321-335. doi: 10.1080/07391102.2018.1426497
33. Fotouhi L, Hashkavayi AB, Heravi MM. Interaction of sulfadiazine with DNA on a MWCNT modified glassy carbon electrode: determination of DNA. International Journal of Biological Macromolecules 2013; 53: 101-106. doi: 10.1016/j.ijbiomac.2012.11.021
34. Islam MM, Moyon NS, Gashnga PM, Mitra S. Interaction of sulfadiazine with model water soluble proteins: a combined fluorescence spectroscopic and molecular modeling approach. Journal of Fluorescence 2014; 24: 579-588. doi: 10.1007/s10895-013-1330-7
35. Zoppi A, Delrivo A, Aiassa V, Longhi MR. Binding of sulfamethazine to β-cyclodextrin and methyl-β-cyclodextrin. American Association of Pharmaceutical Scientists 2013; 14: 727735. doi: 10.1208/s12249-013-9958-9
36. Mascini M, Bagni G, Di Pietro ML, Ravera M, Baracco S et al. Electrochemical biosensor evaluation of the interaction between DNA and metallo-drugs Biometals 2006; 19: 409-418. doi: 10.1007/s10534-005-4340-3
37. Aleksić MM, Kapetanovic V. An overview of the optical and electrochemical methods for detection of DNA – drug interactions. Acta Chimica Slovenica 2014; 61: 555-573.
38. Zhao J, Zheng X, Xing W, Huang J, Li G. Electrochemical studies of camptothecin and its interaction with human serum albumin. International Journal of Molecular Sciences 2007; 8: 42-50. doi: 10.3390/i8010042
39. Omanović D, Branica M. Automation of voltammetric measurements by polarographic analyser PAR 384B. Croatica Chemica Acta 1998; 71: 421-433.
40. Wavefunction, Inc. Spartan08 for Windows. Irvine, CA, USA: Wavefunction, Inc., 2008
41. Frisch MJ, Trucks GW, Schlegel HB, Scuseria GE, Robb MA et al. Gaussian 09 C.01. Wallingford, CT, USA: Gaussian, Inc., 2009.
42. Kohn W, Sham LJ. Self-consistent equations including exchange and correlation effects. Physical Review 1965; 140: A1133-A1138. doi: 10.1103/PhysRev.140.A1133
43. Becke AD. Density-functional exchange-energy approximation with correct asymptotic behavior. Physical Review A 1988; 38: 3098-3100. doi: 10.1103/PhysRevA.38.3098

44. Becke AD. Density-functional thermochemistry. III. The role of exact exchange. Journal of Chemical Physics 1993; 98: 5648-5652. doi: 10.1063/1.464913

45. Chai JD, Head-Gordon M. Long-range corrected hybrid density functionals with damped atom–atom dispersion corrections. Physical Chemistry Chemical Physics 2008; 10: 6615-6620. doi: 10.1039/B810189B

46. Dennington R, Keith T, Millam J. GaussView 5.0.9 Shawnee Mission, KS, USA: Semichem, Inc., 2009.

47. Lee C, Yang W, Parr RG. Development of the Colle-Salvetti correlation-energy formula into a functional of the electron density. Physical Review B 1988; 37: 785-789. doi: 10.1103/PhysRevB.37.785

48. Tomasi J, Mennucci B, Cancès E. The IEF version of the PCM solvation method: an overview of a new method addressed to study molecular solutes at the QM ab initio level. Journal of Molecular Structure (Theochem) 1999; 464: 211-226. doi: 10.1016/S0166-1280(98)00553-3

49. Bellú S, Hure E, Trapé M, Rizotto M. The interaction between mercury(II) and sulfathiazole. Quimica Nova 2003; 26: 188-192. doi: 10.1590/S0100-40422003000200008

50. Bashammakh AS. Differential pulse-adsorptive cathodic stripping voltammetric determination of sulfadiazine drug in pharmaceutical formulations and drug residue in wastewater at a hanging mercury dropping electrode. Arabian Journal for Science and Engineering 2017; 42: 183-192. doi: 10.1007/s13369-016-2195-2

51. Hills GJ. Electrochemistry, Vol. 3. London, UK: Royal Society of Chemistry, 1973.

52. Cottrell PT, Mann CK. Electrochemical reduction of arylsulfonamides. Journal of the American Chemical Society 1971; 93: 3579-3583. doi: 10.1021/ja00744a006

53. Manousec O, Exner O, Zuman P. Fission activated carbon-nitrogen and carbon-sulphur bonds, XI., Polarographic reduction of substituted benzenesulphonamides. In: Zuman P (editor). Topics in Organic Polarography. London, UK: Plenum Press, 1970, p. 324.

54. Heyrovský M, Mader P, Vavřička S, Veselá V, Fedurco M. The anodic reactions at mercury electrodes due to cysteine. Journal of Electroanalytical Chemistry 1997; 430: 103-117. doi: 10.1016/S0022-0728(97)00103-4

55. Heyrovský M, Vavřička S. Adsorption effects of electroactive species in d.c. polarography demonstrated in the case of the anodic waves of cysteine. Journal of Electroanalytical Chemistry 1997; 423: 125-130. doi: 10.1016/S0022-0728(96)04691-8

56. Gowda BG, Mallappa M, Shivakumar A, Sharma J. Electrochemical and spectroscopic studies on the interaction of ketoconazole with herring sperm DNA. Der Pharma Chemica 2014; 6: 256-264.

57. Harding SE, Rowe AJ. Insight into protein–protein interactions from analytical ultracentrifugation. Biochemical Society Transactions 2010; 38: 901-907. doi: 10.1042/BST0380901

58. Braun-Sand S, Strajbl M, Warshel A. Studies of proton translocations in biological systems: simulating proton transport in carbonic anhydrase by EVB-based models. Biophysical Journal 2004; 87: 2221-2239. doi: 10.1529/biophysj.104.043257

59. Riendeau D, Percival MD, Brideau C, Charleson S, Dube D et al. Etoricoxib (MK-0663): Preclinical Profile and comparison with other agents that selectively inhibit cyclooxygenase-2. Journal of Pharmacology and Experimental Therapeutics 2001; 296: 558-566.

60. Leś A, Adamowicz L, Rode W. Modeling of reaction steps relevant to deoxyuridylate (dUMP) enzymatic methylation and thymidylate synthase mechanism-based inhibition. Journal of Biomolecular Structure Dynamics 1998; 15: 703-715. doi: 10.1080/07391102.1998.10508986

61. Wójcik A, Naumov S, Marciniak B, Hermann R, Brede O. Thiyl radical interaction with pyrimidine C5 − C6 double bond. Journal of Physical Chemistry B 2005; 109: 15135-15144. doi: 10.1021/jp051711s

62. Smith KC, Aplin RT. A mixed photoproduct of uracil and cysteine (5-S-cysteine-6-hydrouracil). A possible model for the in vivo cross-linking of deoxyribonucleic acid and protein by ultraviolet light. Biochemistry 1966; 5: 2125-2130. doi: 10.1021/bi00870a046

63. Cuervo C, González J, Rives V, Vicente MA. Characterization of a sulfadiazine-induced lithiasis calculus by physicochemical techniques. AAPS PharmSciTech 2013; 14: 128-132. doi: 10.1208/s12249-012-9892-2

64. Pawlukojć A, Leciejewicz J, Ramirez-Cuesta AJ, Nowicka-Scheibe J. L-Cysteine: neutron spectroscopy, Raman, IR and ab initio study. Spectrochimica Acta Part A 2005; 61: 2474-2481. doi: 10.1016/j.saa.2004.09.012

65. Parker SF. Assignment of the vibrational spectrum of l-cysteine. Chemical Physics 2013; 424: 75-79. doi: 10.1016/j.chemphys.2013.04.020

66. Gunasekaran S, Bright A, Renuga Devi TS, Arunbalaji R, Anand G et al. Experimental and semi-empirical computations of the vibrational spectra of methionine, homocysteine and cysteine. Archives of Physics Research 2010; 1: 12-26.

67. Oanca G, Stare J, Mavri J. How fast monoamine oxidases decompose adrenaline? Kinetics of isoenzymes A and B evaluated by empirical valence bond simulation. Proteins 2017; 85: 2170-2178. doi: 10.1002/prot.25374

68. Koopmans T. Über die Zuordnung von Wellenfunktionen und Eigenwerten zu den Einzelnen Elektronen Eines Atoms. Physica 1934; 1: 104-113 (in German). doi: 10.1016/S0031-8914(34)90011-2

69. Geerlings P, De Proft F, Langenaeker W. Conceptual density functional theory. Chemical Reviews 2003; 103: 1793-1874. doi: 10.1021/cr990029p

70. Mulliken RS. A new electroaffinity scale; together with data on valence states and on valence ionization potentials and electron affinities. Journal of Chemical Physics 1934; 2: 782-793. doi: 10.1063/1.1749394

71. Pearson RG. Recent advances in the concept of hard and soft acids and bases. Journal of Chemical Education 1987; 64: 561-567. doi: 10.1021/ed064p561

72. Parr RG, Chattaraj PK. Principle of maximum hardness. Journal of the American Chemical Society 1991; 113: 1854-1855. doi: 10.1021/ja00005a072

73. Parr RG, Pearson RG. Absolute hardness: companion parameter to absolute electronegativity. Journal of the American Chemical Society 1983; 105: 7512-7516. doi: 10.1021/ja00364a005

74. Parr RG, von Szentpaly L, Liu S. Electrophilicity-based charge transfer descriptor. Journal of the American Chemical Society 1999: 121: 1922-1924. doi: 10.1021/jp0649549

75. Padmanabhan J, Parthasarathi R, Subramanian V, Chattaraj PK. Electrophilicity-based charge transfer descriptor. Journal of Physical Chemistry A 2007; 111: 1358-1361. doi: 10.1021/jp0649549

Supporting Information

Table S1. Conformer analysis of SD-CYS (NH_2-bridged) in water at ωB97XD/6-311++G(d,p) level.

SD-CYS (NH2-bridged)	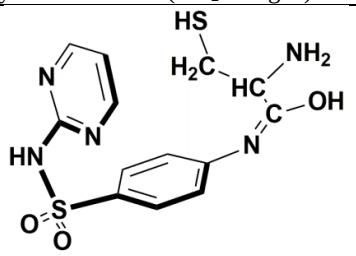	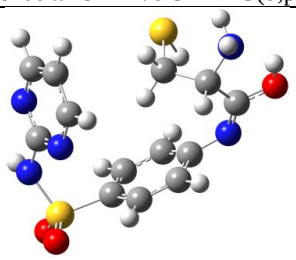 wSDCYS1C57	
Conformers	E+ZPE (a.u.)	Conformers	E+ZPE (a.u.)
wSDCYS1C01	–1799.857619	wSDCYS1C53	–1799.858785
wSDCYS1C02	–1799.857923	wSDCYS1C54	–1799.860172
wSDCYS1C03	–1799.857778	wSDCYS1C55	–1799.853048
wSDCYS1C04	–1799.856394	wSDCYS1C57*	–1799.862079
wSDCYS1C06	–1799.855928	wSDCYS1C58	–1799.853294
wSDCYS1C08	–1799.861613	wSDCYS1C60	–1799.854521
wSDCYS1C09	–1799.857808	wSDCYS1C62	–1799.854614
wSDCYS1C10	–1799.856410	wSDCYS1C64	–1799.850236
wSDCYS1C14	–1799.862024	wSDCYS1C65	–1799.850177
wSDCYS1C16	–1799.854602	wSDCYS1C66	–1799.855575
wSDCYS1C17	–1799.854966	wSDCYS1C68	–1799.854975
wSDCYS1C18	–1799.858853	wSDCYS1C71	–1799.853785
wSDCYS1C20	–1799.855639	wSDCYS1C72	–1799.855175
wSDCYS1C22	–1799.859618	wSDCYS1C73	–1799.850921
wSDCYS1C24	–1799.859775	wSDCYS1C74	–1799.853304
wSDCYS1C25	–1799.857434	wSDCYS1C75	–1799.851125
wSDCYS1C26	–1799.857400	wSDCYS1C76	–1799.858189
wSDCYS1C27	–1799.856527	wSDCYS1C77	–1799.855499
wSDCYS1C28	–1799.855612	wSDCYS1C78	–1799.860584
wSDCYS1C29	–1799.858384	wSDCYS1C80	–1799.858192
wSDCYS1C30	–1799.855519	wSDCYS1C82	–1799.850320
wSDCYS1C32	–1799.854021	wSDCYS1C83	–1799.851978
wSDCYS1C33	–1799.855113	wSDCYS1C84	–1799.851113
wSDCYS1C34	–1799.855670	wSDCYS1C85	–1799.851268
wSDCYS1C36	–1799.854129	wSDCYS1C86	–1799.855703
wSDCYS1C37	–1799.854129	wSDCYS1C88	–1799.855277
wSDCYS1C38	–1799.856958	wSDCYS1C90	–1799.857155
wSDCYS1C40	–1799.856226	wSDCYS1C91	–1799.856692
wSDCYS1C42	–1799.853976	wSDCYS1C92	–1799.851112
wSDCYS1C43	–1799.861612	wSDCYS1C93	–1799.854595
wSDCYS1C44	–1799.854291	wSDCYS1C94	–1799.854475
wSDCYS1C45	–1799.855978	wSDCYS1C95	–1799.855486
wSDCYS1C46	–1799.852675	wSDCYS1C96	–1799.855456
wSDCYS1C47	–1799.857649	wSDCYS1C97	–1799.855499
wSDCYS1C48	–1799.852740	wSDCYS1C98	–1799.860584
wSDCYS1C50	–1799.852836	wSDCYS1C99	–1799.851216
wSDCYS1C52	–1799.853001	wSDCYS1C100	–1799.853865

*H2O (E+ZPE): –76.4188; E+ZPE (SD-CYS (NH2-bridged))= –1876.2808 a.u.

Table S2. Conformer analysis of SD-CYS (SH-bridged) in gas phase and in water at ωB97XD/6-311++G(d,p) level.

SD-CYS	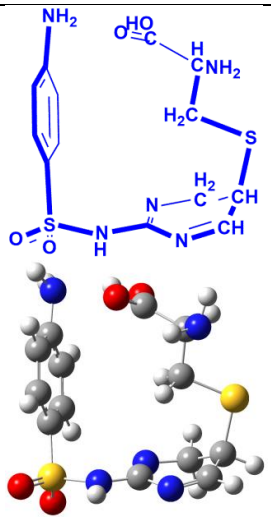 wSDCYS2C26	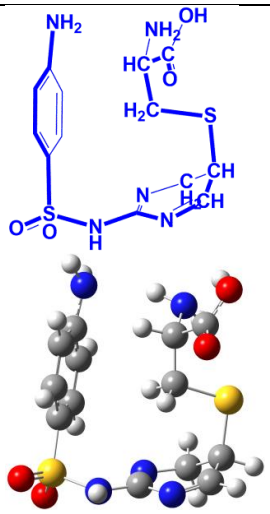 wSDCYS2C21
Conformers	E+ZPE (a.u.) (gas)	E+ZPE (a.u.) (water)
wSDCYS2C01	–1876.245250	–1876.281808
wSDCYS2C02	–1876.250939	–1876.284542
wSDCYS2C04	–1876.249825	–1876.282177
wSDCYS2C06	–1876.245081	–1876.281374
wSDCYS2C08	–1876.249201	–1876.281223
wSDCYS2C09	–1876.250385	–1876.280140
wSDCYS2C10	–1876.240627	–1876.279351
wSDCYS2C12	–1876.244753	–1876.278274
wSDCYS2C13	–1876.244614	–1876.278690
wSDCYS2C14	–1876.250943	–1876.284576
wSDCYS2C15	–1876.247978	–1876.283097
wSDCYS2C16	–1876.254737	–1876.287237
wSDCYS2C17	–1876.245108	–1876.280810
wSDCYS2C18	–1876.245033	–1876.281369
wSDCYS2C20	–1876.247611	–1876.278342
wSDCYS2C21	–1876.251370	–1876.287711
wSDCYS2C22	–1876.247428	–1876.278336
wSDCYS2C24	–1876.247802	–1876.281786
wSDCYS2C25	–1876.247802	–1876.281786
wSDCYS2C26	–1876.252282	–1876.283502
wSDCYS2C27	–1876.244929	–1876.278333
wSDCYS2C28	–1876.251861	–1876.283071
wSDCYS2C29	–1876.244858	–1876.278391
wSDCYS2C30	–1876.248975	–1876.277174
wSDCYS2C31	–1876.243325	–1876.281114
wSDCYS2C32	–1876.252270	–1876.281741
wSDCYS2C33	–1876.247329	–1876.277994
wSDCYS2C34	–1876.249820	–1876.280965
wSDCYS2C36	–1876.244971	–1876.278228
wSDCYS2C38	–1876.241995	–1876.279783
wSDCYS2C39	–1876.251080	–1876.282796
wSDCYS2C40	–1876.245949	–1876.279683
wSDCYS2C41	–1876.246214	–1876.278817

wSDCYS2C43	–1876.242300	–1876.276294
wSDCYS2C44	–1876.245873	–1876.279503
wSDCYS2C45	–1876.245217	–1876.275756
wSDCYS2C46	–1876.243729	–1876.279334
wSDCYS2C47	–1876.242291	–1876.275978
wSDCYS2C48	–1876.248068	–1876.281679
wSDCYS2C50	–1876.242279	–1876.276150
wSDCYS2C51	–1876.247367	–1876.278433
wSDCYS2C52	–1876.237486	–1876.273056
wSDCYS2C54	–1876.244759	–1876.276291
wSDCYS2C56	–1876.245878	–1876.278227
wSDCYS2C57	–1876.243229	–1876.278256
wSDCYS2C58	–1876.243668	–1876.276064
wSDCYS2C60	–1876.244689	–1876.276322
wSDCYS2C61	–1876.254601	–1876.281337
wSDCYS2C62	–1876.244645	–1876.279405
wSDCYS2C63	–1876.243364	–1876.280340
wSDCYS2C64	–1876.244483	–1876.279343
wSDCYS2C65	–1876.241987	–1876.277654
wSDCYS2C66	–1876.248145	–1876.280694
wSDCYS2C68	–1876.243870	–1876.277703
wSDCYS2C70	–1876.242973	–1876.276251
wSDCYS2C71	–1876.248077	–1876.281679
wSDCYS2C72	–1876.238488	–1876.273787
wSDCYS2C73	–1876.239125	–1876.274895
wSDCYS2C74	–1876.243611	–1876.279408
wSDCYS2C75	–1876.248083	–1876.282149
wSDCYS2C76	–1876.247909	–1876.276172
wSDCYS2C77	–1876.238480	–1876.273883
wSDCYS2C78	–1876.243164	–1876.275422
wSDCYS2C80	–1876.247349	–1876.276365
wSDCYS2C81	–1876.239416	–1876.278313
wSDCYS2C82	–1876.245977	–1876.279702
wSDCYS2C83	–1876.246466	–1876.280162
wSDCYS2C84	–1876.242857	–1876.275697
wSDCYS2C85	–1876.236861	–1876.279109
wSDCYS2C86	–1876.237456	–1876.279115
wSDCYS2C87	–1876.246329	–1876.277570
wSDCYS2C88	–1876.244460	–1876.277436
wSDCYS2C89	–1876.243652	–1876.277075
wSDCYS2C90	–1876.238715	–1876.276802
wSDCYS2C92	–1876.247477	–1876.279228
wSDCYS2C93	–1876.239962	–1876.273273
wSDCYS2C94	–1876.247904	–1876.280247
wSDCYS2C95	–1876.236688	–1876.279109
wSDCYS2C96	–1876.243396	–1876.278041
wSDCYS2C97	–1876.245574	–1876.274370
wSDCYS2C98	–1876.244372	–1876.276286
wSDCYS2C99	–1876.241391	–1876.272381
wSDCYS2C100	–1876.244291	–1876.277273

Table S3. Dipole moments (μ), sum of total electronic energies and zero point energies (E+ZPE), sum of electronic energies and free energies (E+ΔG, Hartree), complexation energy (ΔE), complexation free energy changes (ΔΔG), and selected geometrical parameters of investigated compounds calculated at ωB97XD/6-311++G(d,p) level in water

	CYS	SD	SD-CYS S-bridge
μ (D)	6.22	11.2	16.7
E+ZPE (Hartree)	–721.8535	–1154.4459	–1876.2877
E+ΔG (Hartree)	–721.8864	–1154.4889	–1876.3401
[a]ΔE (kcal/mol)			7.34
[b]ΔΔG (kcal/mol)			22.09
Distances (Å)			
C2-S1		1.758	1.761
S1-N1		1.681	1.676
N1-C3		1.392	1.393
S2-C7	1.828	-	1.830
C7-C8	1.529	-	1.528
C5-S2	-	-	1.834
Angles (°)			
C2-S1-N1	-	106.64	106.43
S1-N1-C3	-	125.41	124.62
S2-C7-C8	114.12	-	109.75
Dihedral angles (φ°)			
C1-C2-S1-N1	-	74.74	96.84
C2-S1-N1-C3	-	49.88	–53.32
S1-N1-C3-N3	-	–159.64	–15.15
S1-N1-C3-N2	-	21.07	165.52
N1-C3-N3-C6	-	–178.73	179.89
N1-C3-N2-C4	-	179.48	–166.60
N2-C4-C5-S2	-	-	103.02
C4-C5-S2-C7	-	-	–64.06

[a]: ΔE = [E+ZPE(SD-CYS) – E+ZPE(SD) – E+ZPE(CYS)].
[b]: ΔΔG = [E+ΔG(SD-CYS) - E+ΔG(SD) - E+ΔG(CYS)].

Table S4. Selected vibrational frequencies (cm^{-1}) of SD-CYS, CYS, and SD at ground state by ωB97XD method with 6-311++G(d,p) basis set.

(cm^{-1})	SD-CYS 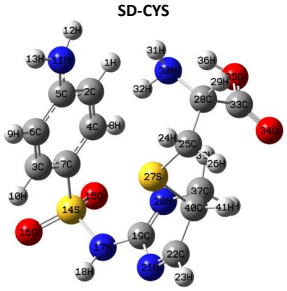		I	(cm^{-1})	SD 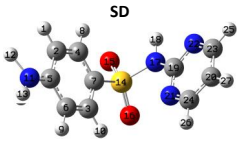		I	(cm^{-1})	CYS 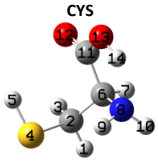		I
3704 (3422)exp	1:ν_{as} (NH2) (aniline)	N(11)-H(12)-H(13)	62.01	3730	ν_{as} (NH2)	N(11)-H(12)-H(13)	62.96	3642	ν_{as} (NH2)	N(8)-H(9)-H(10)	45.30
3624	2:ν (N-H)	N(17)-H(18)	193.20	3619	ν (N-H)	N(17)-H(18)	186.23				
3600 (3353)exp	1:ν_s (NH2) 3:ν_{as} (NH2)	N(11)-H(12)-H(13) (an) N(30)-H(31)-H(32) (cys)	156.60	3616	ν_s (NH2)	N(11)-H(12)-H(13)	118.45	3540	ν_s (NH2)	N(8)-H(9)-H(10)	14.16
3512	3:ν_s (NH2)	N(30)-H(31)-H(32) (cys)	137.74					3416	ν (O-H)	N(13)-H(14)	704.75
								3171	ν_{as} (CH2)	C(2)-H(1)-H(3)	3.23
3363	4:ν (O-H)	N(35)-H(36)	827.36	3246	ν (C-H)	C(20)-H(27)	4.00	3110	ν_s (CH2)	C(2)-H(1)-H(3)	20.67
3203	8:ν (C-H)	C(2)-H(1) (an)	8.55					3076	ν (C-H)	C(6)-H(7)	10.11
3168	7:ν_{as} (CH2)	C(25)-H(24)-H(26) (cys)	7.02	3238	ν (C-H)	C(3)-H(10)	2.39	2740	ν (S-H)	S(4)-H(5)	0.52
3113	5:ν_{as} (CH2)	C(37)-H(38)-H(39) (pyr)	22.14	3215	ν (C-H) ν (C-H)	C(4)-H(8) C(2)-H(1)	6.01	1826	ν (C=O) ρ (O-H)	C(11)-O(12) O(13)-H(14)	1372.40
3040	5:ν_s (CH2)	C(37)-H(38)-H(39)	65.08	3202	ν (C-H)	C(24)-H(26)	26.67	1648	δ (NH2)	N(8)-H(9)-	154.13

(2819)exp		(pyr)								H(10)	
1824	9:ν (C=O) 4:ρ (O-H)	C(33)-O(34) O(35)-H(36)	1467.82	3199	ν (C-H)	C(23)-H(25)	25.60	1450	δ (CH2)	C(2)-H(1)-H(3)	113.46
1756 (1621)exp	11:ν (C=N) 14:ν (C=N) 2:ρ (N-H)	N(20)-C(19) (pyr) N(21)-C(22) (pyr) N(17)-H(19)	1078.23	3198	ν (C-H)	C(6)-H(9)	14.66	1424	ρ (O-H)	O(13)-H(14)	1727.40
1698	14:ν (C=N)	N(21)-C(22) (pyr)	304.05	1668	δ (NH2)	N(11)-H(12)-H(13)	1569.83	1405	ρ (C-H)	C(6)-H(7)	101.78
1671	1:ν_s (CH2)	N(11)-H(12)-H(13) (an)	979.72	1651	ν (C-N) ν (C=C) ν (N-H)	C(19)-N(21) C(24)-C(20) N(17)-H(18)	607.31	1340	ω (CH2)	C(2)-H(1)-H(3)	143.16
1642	8:ν (C=C)	C(2)-C(5) (phen) C(4)-C(7)	65.64	1639	ν (C=C)	C(5)-C(6) C(4)-C(7)	78.74	1241	ν (C-O)	C(11)-O(13)	72.82
1546	ν (C-N) 8:ρ (C-H) ρ (C-H) ρ (C-H) ρ (C-H)	C(5)-N(11) C(6)-H(9) C(3)-H(10) C(2)-H(1) C(4)-H(8)	241.24	1501	ρ (N-H) ρ (C-H) ρ (C-H)	N(17)-H(18) C(20)-H(27) C(24)-H(26)	404.04	1163	τ (NH2)	N(8)-H(9)- H(10)	48.81
1488	7:δ (CH2)	C(25)-H(24)-H(26)	74.87	1486	ν (C=C)	C(3)-C(6) C(2)-C(4)	161.90	1065	ρ (S-H) ρ (C-H)	S(4)-H(5) C(6)-H(7)	242.76
1478 (1383)exp	5:δ (CH2)	C(37)-H(38)-H(39)	27.23	1480	ν (C-N) ρ (C-H) ρ (N-H)	C(19)-N(17) C(24)-H(26) N(17)-H(18)	2163.37	976	ρ (S-H)	S(4)-H(5)	156.56
1454	2:ρ (N-H)	N(17)-H(18)	1711.92	1428	ρ (N-H) ρ (C-H)	N(17)-H(18) C(23)-C(20)	97.22	910	ρ (O-H) ω (CH2)	O(13)-H(14) N(8)-H(9)- H(10)	566.24
1437	4:ρ (O-H) cys	O(35)-H(36)	2104.92	1360	ρ (N-H) ρ (C-H)	C(24)-H(26) N(17)-H(18)	79.29	877	ρ (O-H) ω (CH2)	O(13)-H(14) N(8)-H(9)- H(10)	1082.98
1333	ν (C-N) 8:ρ (C-H) 8:ρ (C-H)	C(5)-N(11) C(4)-H(8) C(2)-H(1)	403.47	1348	ν (C-N)	C(5)-N(11) C(4)-H(8) C(2)-H(1)	484.65	854	ρ (S-H) ν (C-O)	S(4)-H(5) C(11)-O(13)	100.29
1326 (1298)exp	13:ρ (C-H) 5:ρ (C-H)	C(40)-H(41) C(37)-H(38)	213.62	1329	ν_{as} (SO2) ρ (C-H)	S(14)-O(15)-O(16) C(23)-H(25)	1022.81				

1248	2:ρ (N-H) 13:ρ (C-H)	N(17)-H(18) C(40)-H(41)	104.28	1256	ν (C=N) ν (C=C) ρ (N-H)	C(19)-N(22) C(24)-C(20) N(17)-H(18)	112.85				
1150 (1151)exp	10:ν_s (SO2) 2:ρ (N-H)	S(14)-O(15)-O(16) N(17)-H(11)	2357.14	1152	ν_s (SO2) ρ (C-H)	S(14)-O(15)-O(16) C(4)-H(8)	2689.11				
				946	ν (S-N)	S(14)-N(17)	934.79				
				862	ω (C-H) ω (C-H) ω (C-H) ω (C-H) ν (S-N)	C(2)-H(1) C(4)-H(8) C(3)-H(10) C(6)-H(9) S(14)-N(17)	893.98				
				831	ω (C-H) ω (C-H) ω (C-H)	C(23)-H(25) C(24)-H(26) C(20)-H(27)	368.96				
				679	ν (S-C)	S(14)-C(7)	771.36				
				568	ω (SO2)	S(14)-O(15)-O(16)	2399				

ν: Stretching; δ: in-plane scissoring; ρ: in-plane rocking; τ: out-of-plane twisting; ω; out-of-plane wagging; s:symetrical; as: asymetrical.
Exp: Experimental; phen: pheyl; an: aniline; cys: cysteine; pyr: primidine; predicted vibrational frequencies were not scaled down with a factor.

Table S5. Vertical excitation energies (ΔE) corresponding to wavelengths (λ_{ex}), transition dipole moments (μ_{tr}), oscillator strengths (f), excitation character, and involved transition molecular orbitals and their percentage contributions for SD in water at B3LYP/6-311++G(d,p) level.

State	ΔE (eV)	λ_{ex} (nm)	μ_{tr} (D)	f	Character[a]	Predominant transitions	%
S_1	4.04	307	0.2874	0.0285	ICT1	H→L	70
S_2	4.47	277	0.0034	0.0004	LE1, ICT1 LE1, ICT1	H-2→L H-3→L	58 33
S_3	4.58	271	1.7280	0.1940	LE2, ICT1	H→L+1	65
S_4	4.69	265	0.2399	0.0275	LE2	H→L+3	63
S_5	4.95	251	1.9220	0.2329	ICT1, LE1, LE2	H→L+2	63
S_6	4.97	249	0.4558	0.0556	LE1, ICT1	H-1→L	65
S_7	5.14	241	0.1218	0.0027	LE1, LE2 LE1, LE2	H-2→L+1 H-2→L+2	46 37
S_{10}	5.53	224	0.9632	0.1304	ICT2, LE1	H-1→L+1	65
S_{14}	5.87	211	0.3463	0.0498	LE1, LE2	H-3→L+1	58
S_{16}	5.96	208	1.0497	0.1532	ICT2, LE1	H-1→L+2	58
S_{18}	6.07	204	0.4223	0.0628	ICT2, LE2	H-2→L+3	62
S_{20}	6.17	201	0.6430	0.0972	LE1, LE2	H-2→L+2	57

[a] ICT1: Intramolecular charge transfer from aniline to pyrimidine; LE1: local excitation of pyrimidine; LE2: local excitation of aniline; ICT2: intramolecular charge transfer from pyrimidine to aniline.

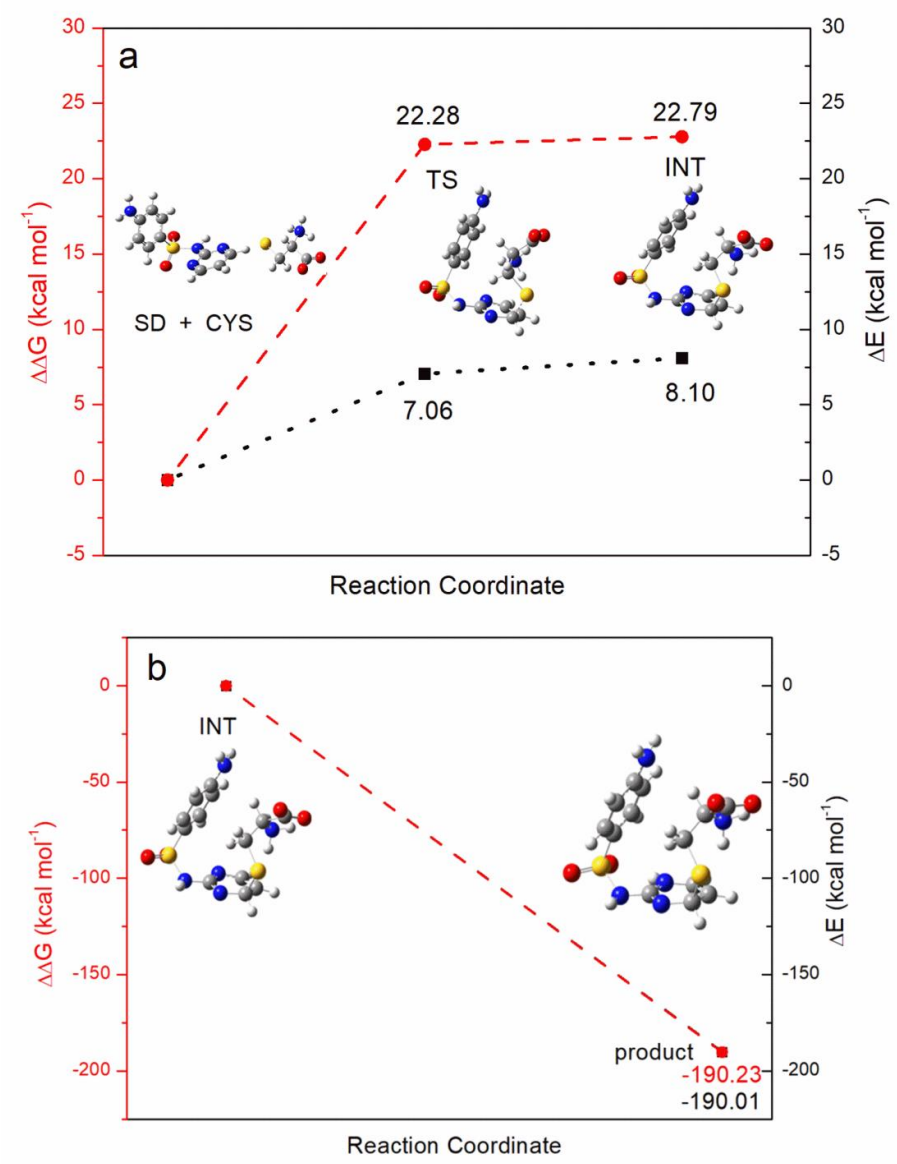

Figure S1. Calculated electronic (ΔE) and free energy (ΔΔG) differences for the steps: a) formation of INT from SD and CYS and b) formation of the product from INT.

	SD	SD-CYS
	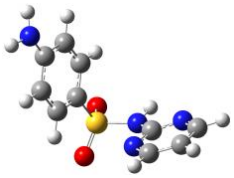	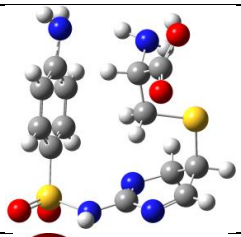
LUMO+5	-	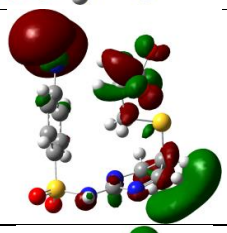
LUMO+3	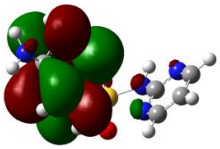	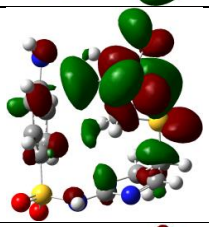
LUMO+2	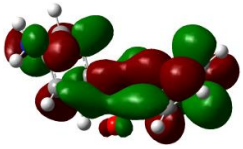	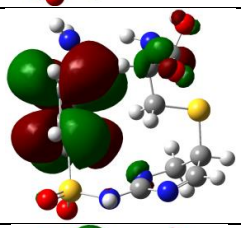
LUMO+1	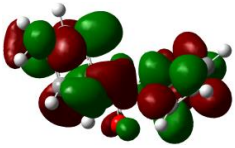	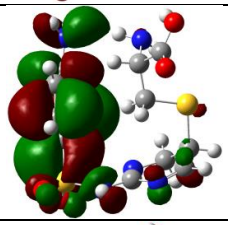
LUMO	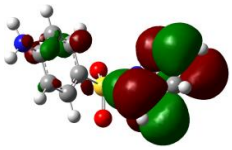	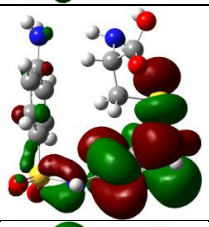
HOMO	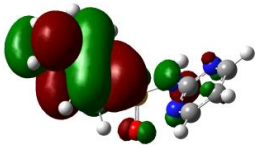	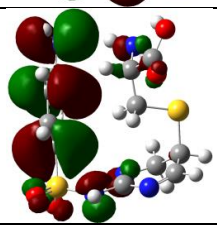

HOMO-1	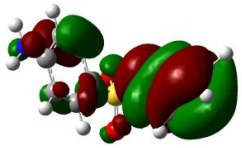	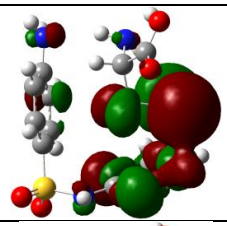
HOMO-2	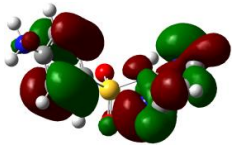	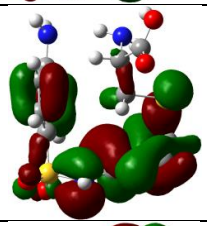
HOMO-3	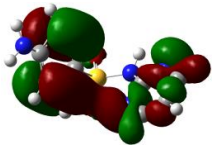	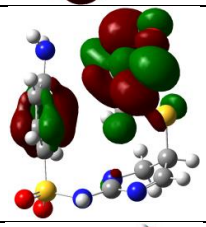
HOMO-4	-	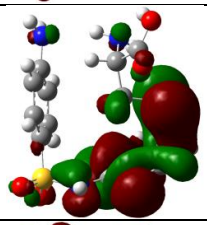
HOMO-8	-	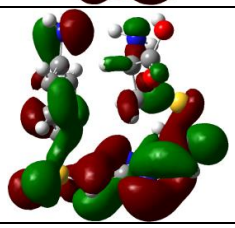

Figure S2. Selected molecular orbitals of SD and SD-CYS complex in water calculated with B3LYP/6-311++G(d,p).